HHS Public Access

Author manuscript

Cell Host Microbe. Author manuscript; available in PMC 2019 November 14.

Published in final edited form as:

Cell Host Microbe. 2018 November 14; 24(5): 703–716.e3. doi:10.1016/j.chom.2018.10.009.

Broadly neutralizing antibodies against HCV use a CDRH3 disulfide motif to recognize an E2 glycoprotein site that can be targeted for vaccine design

Andrew I. Flyak[1], **Stormy Ruiz**[1], **Michelle Colbert**[2], **Tiffany Luong**[1], **James E. Crowe Jr.**[3,4,5], **Justin R. Bailey**[2,*], and **Pamela J. Bjorkman**[1,*]

[1]Division of Biology and Biological Engineering, California Institute of Technology, Pasadena, CA, 91125, USA.

[2]Department of Medicine, Johns Hopkins University School of Medicine, Baltimore, MD, 21205, USA.

[3]Department of Pathology, Microbiology and Immunology, Vanderbilt University Medical Center, Nashville, TN, 37232, USA.

[4]Department of Pediatrics, Vanderbilt University Medical Center, Nashville, TN, 37232, USA.

[5]Vanderbilt Vaccine Center, Vanderbilt University Medical Center, Nashville, TN, 37232, USA.

SUMMARY

Hepatitis C virus (HCV) vaccine efforts are hampered by extensive genetic diversity of HCV envelope glycoproteins E1 and E2. Structures of broadly neutralizing antibodies (bNAbs) (e.g., HEPC3, HEPC74) isolated from individuals who spontaneously cleared HCV infection facilitate immunogen design to elicit antibodies against multiple HCV variants. However, challenges in expressing HCV glycoproteins previously limited bNAb-HCV structures to complexes with truncated E2 cores. Here we describe crystal structures of full-length E2 ectodomain complexes

*Co-corresponding authors, Justin R. Bailey. Johns Hopkins University School of Medicine, Rangos Research Building, Suite 520, Baltimore, MD 21205. Phone: (410) 614-6087. Fax: (410) 614-9775, jbailey7@jhmi.edu, Pamela J. Bjorkman. Division of Biology and Biological Engineering, California Institute of Technology, 1200 E. California Blvd., Pasadena, CA 91125. Phone: (626) 395-8350. Fax: (626) 792-3683, bjorkman@caltech.edu.

AUTHOR CONTRIBUTIONS

A.I.F., J.R.B., and P.J.B. conceived the study; A.I.F. and S.R. optimized the crystallography conditions; A.I.F. solved and analyzed the crystal structures; T.L. expressed and purified proteins; S.R. performed ELISA experiments; M.C. performed neutralization experiments; J.E.C. provided antibody sequences; A.I.F., S.R., M.C., J.R.B., J.E.C., and P.J.B. analyzed the data; A.I.F. and P.J.B. wrote the original draft; all authors reviewed and edited the manuscript.

DECLARATION OF INTERESTS

A.I.F., J.E.C., and J.R.B. are inventors of patents submitted pertaining to some of the antibodies and antigens presented in this paper. J.E.C. has served as a consultant for Takeda Vaccines, Sanofi Pasteur, Pfizer, and Novavax, is on the Scientific Advisory Boards of CompuVax, GigaGen, Meissa Vaccines, PaxVax, and is Founder of IDBiologics, Inc. The other authors declare no competing interests.

DATA AND SOFTWARE AVAILABILITY

Coordinates for atomic models are deposited in the Protein Data Bank under the accession numbers 6MED (HEPC3), 6MEE (HEPC74), 6MEF (AR3C), 6MEG (HEPC46), 6MEH (HEPC74-E2ecto), 6MEI (HEPC3-E2ecto), 6MEJ (HEPC3-E2ecto-HEPC46), and 6MEK (HEPC3-E2core-HEPC46).

with HEPC3 and HEPC74, revealing lock-and-key antibody-antigen interactions, E2 regions (including a target of immunogen design) that were truncated or disordered in E2 cores, and an antibody CDRH3 disulfide motif that exhibits common interactions with a conserved epitope despite different bNAb-E2 binding orientations. The structures display unusual features relevant to common genetic signatures of HCV bNAbs and demonstrate extraordinary plasticity in antibody-antigen interactions. In addition, E2 variants that bind HEPC3/HEPC74-like germline precursors may represent candidate vaccine immunogens.

Graphical Abstract

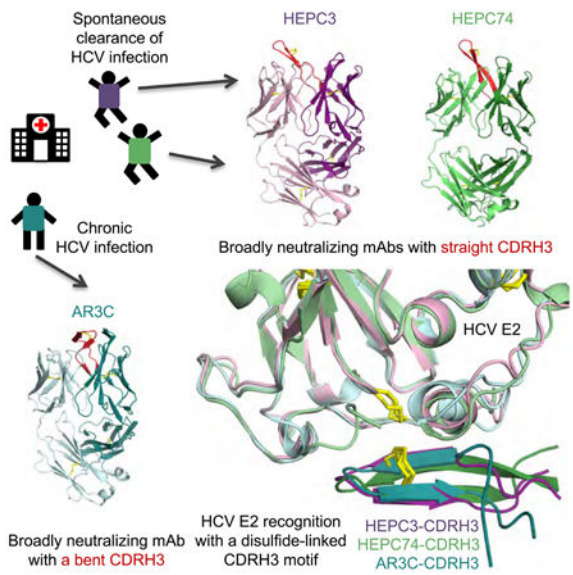

eTOC blurb

Flyak et al. present the structures of full-length E2 ectodomains of HCV bound to two broadly neutralizing antibodies isolated from individuals who spontaneously cleared infection. The structures illustrate shared genetic signatures and a common mode of antigen recognition using CDRH3s. These results demonstrate antibody plasticity and inform lineage-targeted immunogen design.

Keywords

Broadly neutralizing antibodies; structure; HCV; E2; glycoprotein; epitope; disulfide bond

INTRODUCTION

Worldwide, more than 70 million people are infected with hepatitis C virus (HCV) and half a million die every year, mostly from cirrhosis or hepatocellular carcinoma, the most common type of liver cancer. HCV is a blood-borne pathogen that is transmitted mainly through injection drug use. The recent increase in the incidence of HCV infection in the United States is linked to increasing rates of opioid addiction, especially among young Americans (Zibbell et al., 2018). Despite the recent approval of direct-acting antivirals

(DAAs), identification of HCV-infected individuals remains challenging (Denniston et al., 2012). Furthermore, the high cost of treatment and the possibility of reinfection after successful treatment suggest that HCV eradication is likely to be achieved only with a prophylactic vaccine (Rosen, 2017).

The development of an effective HCV vaccine has been challenging primarily due to the enormous genetic diversity of HCV, which has been estimated to be higher than that of HIV-1 (Yusim et al., 2010). However, in contrast to HIV-infected individuals who do not clear their infections, approximately 25% of individuals who become infected with HCV are able to clear the infection spontaneously (Micallef et al., 2006). We and others have shown that spontaneous clearance of HCV infection is associated with the early appearance of bNAbs that bind to HCV envelope proteins (E1 and E2) and neutralize multiple HCV variants (Bailey et al., 2017; Osburn et al., 2014; Pestka et al., 2007).

The HCV genome encodes a single polyprotein of about 3,010 amino acids, which is processed by viral and cellular proteases into ten gene products (Figure S1A). The N-terminal region of the HCV polyprotein encodes two structural proteins: E1 (residues 192–383) and E2 (residues 384–746). E1 and E2 are heavily glycosylated type I transmembrane proteins that associate to form a noncovalent heterodimer – E1E2 (Freedman et al., 2016). The role of E1 in the viral cycle remains poorly understood, and only a few E1-specific human bNAbs are described in the literature (Meunier et al., 2008). HCV E2 is the primary target of potent bNAbs and mediates viral entry into the host cell by interacting with multiple receptors on the cell surface including tetraspanin CD81, scavenger receptor-B1, claudin, and occludin (Zeisel et al., 2011). Structural studies of E1 and E2 have been hindered by difficulties in the expression of soluble ectodomains (Khan et al., 2015). However, crystal structures of a truncated E2 core construct (E2core) lacking flexible regions such as hypervariable domain 1 (HVR1), antigenic site 412 (AS412; residues 412–423), and variable region 2 (VR2; residues 460–485), revealed a central ß-sandwich flanked by front (residues 424–459) and back (residues 597–645) layers (Khan et al., 2014; Kong et al., 2013) (Figure S1B). Most bNAbs to HCV map to the conserved but flexible CD81-binding site (CD81bs), which comprises the AS412 region, the front layer, and the CD81 binding loop (residues 519–535). The CD81bs-specific bNAbs HCV1, AP33, HC33.1, and 3/11 recognize the AS412 region, while the AR3A, AR3B, AR3C, AR3D, HC84–1, and HC84–27 bNAbs recognize the highly-conserved E2 front layer (Deng et al., 2013; Gopal et al., 2017; Kong et al., 2013; Kong et al., 2012a; Kong et al., 2012b; Krey et al., 2013; Li et al., 2015; Meola et al., 2015; Potter et al., 2012). Two other bNAbs, AR4A and AR5A, bind to E1E2 conformational epitopes, sharing critical residues at the C-terminus of E2 and requiring complexed E1 and E2 for binding (Giang et al., 2012). Structural information regarding bNAb recognition of HCV E2 is limited to the structure of AR3C, a phage display-isolated antibody (Law et al., 2008), bound to an E2 core construct, raising the question of how diverse bNAbs capture this dynamic region in the context of the an intact E2 ectodomain (Kong et al., 2016).

Here we present structures of two E2 front layer-specific bNAbs, HEPC3 and HEPC74, which we isolated from individuals who spontaneously cleared HCV (Bailey et al., 2017). These bNAbs use the same germline heavy chain gene segments and exhibit a limited

number of somatic mutations. We describe a shared disulfide-stabilized β-turn motif at the tip of heavy chain complementarity determining region 3 (CDRH3) that is partially encoded by a common germline D gene and resembles a motif in AR3C (Kong et al., 2013). Crystal structures of unliganded HEPC3, HEPC74, and AR3C Fabs showed that their CDRH3 loops adopt different orientations within their Fab combining sites despite presentation of the common disulfide motif, and crystal structures of HEPC3 and HEPC74 in complex with HCV E2 revealed a new binding orientation for a bNAb recognizing the E2 front layer. Comparisons with the AR3C-E2core structure (Kong et al., 2013) show that HEPC3 and HEPC74 uses a different engagement mode to allow the common disulfide-stabilized β-turn motif in CDRH3 to recognize the same epitope, highlighting the importance of this motif in recognition of the conserved E2 epitope and demonstrating the plasticity of antibody combining sites to use their CDRH3 loops in a common mode of HCV antigen recognition. In addition, we used new expression and purification techniques to produce bNAb complexes with full-length E2 ectodomains (E2ecto) for structural studies, revealing the conformations of previously-disordered or truncated regions of E2 including the AS412 region and VR2 loop. We show that the AS412 region, a target for epitopebased vaccine design (Kong et al., 2015), adopts at least two distinct conformations even when bound to a single bNAb. Taken together, the identification of common genetic signatures used by potent bNAbs isolated from different individuals will facilitate lineage-targeted immunogen design to raise bNAbs against the conserved epitope in the HCV E2 front layer.

RESULTS

E2 front layer-specific bNAbs share a common disulfide-linked CDRH3 motif

We recently described a panel of bNAbs isolated from individuals who spontaneously cleared HCV infection. Three of the most potent bNAbs (HEPC3, HEPC43, and HEPC74) were mapped by alanine-scanning mutagenesis to recognize a conserved epitope in the front layer of E2 (Bailey et al., 2017). By analyzing the sequences of front layer-specific bNAbs, including the previously-described human AR3C bNAb (Law et al., 2008), we found that HEPC3, HEPC74 and AR3C shared common sequence signatures (Figure 1A). First, HEPC3, HEPC74, and AR3C are encoded by the same heavy chain variable gene segment, *V_H1–69* (Figure 1A,B), which is frequently used by human bNAbs that target conserved regions on E2 (Bailey et al., 2017; Kong et al., 2013; Krey et al., 2013). Second, despite being isolated from different individuals, these bNAbs share a sequence signature in the third complementarity determining region of the heavy chain (CDRH3) in which a positively-charged amino acid (arginine in HEPC3 and AR3C; lysine in HEPC74) is followed by a tyrosine, and two flanking cysteines separated by four residues, three of which are glycines (R/K-Y-C-G-G-G-X-C motif) (Figure 1A). The cysteines in the HEPC3 and HEPC74 CDRH3 regions are germline-encoded in the human D gene segment 15 (IGHD2–15) (Figure 1B–1C and Figure S2B). In the case of AR3C, one or both cysteine residues are encoded by members of the IGHD2 gene family, either IGHD2–21 or IGHD2–15 (Figure 1B; S2C), and the CDRH3 cysteines form a disulfide bridge that stabilized a β-hairpin-like structure in a crystal structure of ARC3C bound to an E2core protein (Figure 2A) (Kong et al., 2013).

To determine whether CDRH3s of HEPC3 and HEPC74 contain a disulfide-stabilized βhairpin motif, we solved crystal structures of unliganded antigen-binding fragments (Fabs) of these bNAbs (Table S1). The 2.1 Å HEPC3 and 1.4 Å HEPC74 structures revealed that the CDRH3s of both bNAbs form ß-hairpins stabilized by a disulfide bridge (Figure 1D). However, the CDRH3s in these bNAbs were oriented differently than the AR3C disulfide-bonded CDRH3: the HEPC3 and HEPC74 CDRH3s were relatively straight β-hairpins pointing towards the Fab light chain, whereas the AR3C CDRH3 in the AR3C-E2core complex structure bent away from the light chain and towards the CDRH2 (Kong et al., 2013). To address whether the difference in the AR3C CDRH3 conformation reflected changes induced upon antigen binding, we solved a 2.9 Å structure of unliganded AR3C Fab to compare with the unliganded HEPC3 and HEPC74 Fab structures (Figure 1D). Superimposition of unbound and bound forms of AR3C Fab revealed no major changes between the relative positions of the CDRH loops (root mean square deviation, rmsd, for superposition of 124 Cα atoms in bound and unbound AR3C variable heavy (V_H) domains = 0.8 Å); thus the AR3C CDRH3 loop adopted the same bent conformation in both the unliganded Fab and the Fab bound to the E2core (Kong et al., 2013) (Figure S3B).

HEPC3 and HEPC74 recognize HCV E2 using a disulfide-linked CDRH3 motif

The different conformations of the CDHR3s in three *V_H1–69*–encoded bNAbs (straight in HEPC3 and HEPC74; bent in AR3C) resulted in different presentations of the R(K)-Y-C-G-GG-X-C motif, raising the question of how the new bNAbs interact with the conserved epitope in the front layer of HCV E2. To address this question, we determined the structures of HEPC3 bound to an E2 core from the 1a53 strain of HCV ($E2core_{1a53}$) (Figure 2A, Table S2) and HEPC74 bound to an E2 ectodomain from the 1b09 strain of HCV ($E2ecto_{1b09}$) (Figure 2E, Table S2) to compare with the structure of AR3C bound to an E2 core from the 1a154 (H77) strain ($E2core_{1a154}$) (Kong et al., 2013). To facilitate the formation of stable antigen-antibody complexes, we co-expressed the $E2core_{1a53}$ with two E2-binding Fabs: one from HEPC3 and one from the central β-sandwich-specific HEPC46 antibody (Bailey et al., 2017).

The 3.1 Å HEPC3-$E2core_{1a53}$-HEPC46 and 2.0 Å HEPC74-$E2ecto_{1b09}$ structures confirmed alanine scanning mutagenesis results that identified the HEPC3, HEPC74, and HEPC46 epitopes (Bailey et al., 2017). We found that HEPC3, HEPC74, and AR3C have similar binding footprints, sharing multiple contact residues in the front layer and a single contact residue (Trp529) in the CD81 receptor-binding loop (Table S3, S4). Similar to the AR3C-E2core interface (Kong et al., 2013), the HEPC3 and HEPC74 contacts with E2core almost exclusively involve V_H domain residues, burying 1,016 $Å^2$ (HEPC3, 94% of the total Fab buried surface area; BSA) or 1,131 $Å^2$ (HEPC74, 88% of BSA) with the CDRH3 accounting for 43% (HEPC3, 469 $Å^2$) or 40% (HEPC74, 515 $Å^2$) of total BSA on the Fab (Table S3,4). In contrast to the bent CDRH3 conformation in both unliganded and E2-bound AR3C (Figure S3B), the HEPC3 and HEPC74 CDRH3s formed a straight β-hairpin in their free (Figure 1D) and liganded (Figure 2A,E) states, and in common with AR3C, the HEPC3 and HEPC74 V_H domains did not exhibit major rearrangements upon binding to E2 (rmsd for superposition of 124 or 127 Cα atoms in bound and unbound HEPC3 or HEPC74 V_H domains = 0.8 Å or 0.5 Å, respectively) (Figure S3A).

As a result of their different CDRH3 loop conformations, HEPC3/HEPC74 and AR3C bind E2 with different orientations (Figure 3A): when the Fab-E2 structures were aligned on the E2 antigens, the HEPC3 Fab and the HEPC74 Fab were rotated by ~89˚ and ~77 ˚ relative to the AR3C Fab (Figure 3A). This difference in Fab orientation positioned the tips of the HEPC3, HEPC74, and AR3C CDRH3 loops to interact with the same conserved residues in the front layer of E2 (Figure 3B), despite the straight versus bent conformations of their CDRH3s. In all Fabs, the first cysteine residue of the CDRH3 (HEPC3 and HEPC74 – Cys100; AR3C – Cys100A) makes hydrogen bonds with E2 residue Cys429 (Table S3). Although the tips of the HEPC3, HEPC74 and AR3C CDRH3s make the same footprint on the E2 core surface, the difference in Fab approach angles results in different footprints on E2 for the *V_H1–69*–encoded CDRH1 and CDRH2 loops of the bNAbs: HEPC3 and HEPC74's CDRH1 and CDRH2 contact the N-terminus of the E2 α1-helix and the portion of the E2 front layer between the α-helix and variable region 2 (residues 446–448), whereas the AR3C CDRH1 and CDRH2 contact hydrophobic residues on the C-terminus of the α1-helix (Kong et al., 2013) (Figure 3C; Table S3).

The CDRH3 disulfide bond is required for optimal binding and neutralization of HEPC3family bNAbs

To access the functional importance of the CDRH3 disulfide bridge in E2 front layer-specific bNAbs, we replaced the two cysteines in the CDRH3s of HEPC3, HEPC74, and AR3C with either two alanines (2Cys→2Ala mutants) or two serines (2Cys→2Ser mutants) (Figure 4C). The alanine and serine mutants displayed reduced binding to the HCV 1a53 E2 ectodomain ($E2ecto_{1a53}$) by ELISA, with the serine mutants showing the weakest binding (Figure 4A). The mutants also displayed reduced neutralization potencies against the 1a53 HCV strain in an *in vitro* HCV pseudoparticle (HCVpp) neutralization assay (Figure 4A).

To determine the role of the CDRH3 disulfide bond in the evolution of the HEPC3/AR3C family of HCV bNAbs, we evaluated the effects on binding and neutralization potencies of alanine or serine mutations in reverted unmutated ancestor (rua) variants of HEPC3, HEPC74, and AR3C (HEPC3rua, HEPC74rua, and AR3Crua). The RUA variants showed no detectable binding to $E2ecto_{1a53}$ by ELISA, with the exception of the HEPC74rua 2Cys→2Ala mutant, which bound weakly to the 1a53 E2 ectodomain (Figure 4B). Alanine and serine mutants of HEPC3rua, HEPC74rua, and AR3Crua also failed to neutralize the strain 1a53 HCVpp. These data demonstrate the critical role of the CDRH3 disulfide motif for initial germline recognition of HCV by naïve B cells.

Structures of HEPC3 complexes with E2 ectodomains reveal conformations of disordered or truncated regions of E2core

Structural studies of HCV E2 have been complicated by E2 ectodomain proteins forming misfolded disulfide-linked aggregates when overexpressed in eukaryotic cells (Khan et al., 2015). To determine structures of the E2 ectodomain, we developed a method to form stable complexes between an intact E2 ectodomain and one or more Fabs by co-expressing Fab(s) with an E2 ectodomain. This methodology allowed production of stable complexes from which we solved crystal structures of E2 ectodomains from the 1b09 (genotype 1b) and 1a53

(genotype 1a) HCV strains, which were complexed with HEPC3 Fab (HEPC3-E2ecto$_{1b09}$) or with HEPC3 and HEPC46 Fabs (HEPC3-E2ecto$_{1a53}$-HEPC46) (Figure 2C,D, Table S2).

The core regions of the 2.9 Å HEPC3-E2ecto$_{1b09}$ and 2.8 Å HEPC3-E2ecto$_{1a53}$-HEPC46 structures were similar to each other (rmsd = 0.8 Å for superposition of 189 Cα atoms) and to the E2core structures (rmsd = 0.7 Å and 0.9 Å for superposition of 168 Cα atoms between E2ecto$_{1a53}$ /E2core$_{1a53}$ and E2ecto$_{1b09}$ /E2core$_{1a53}$, respectively) (Figure S4). However, the intact ectodomain structures illuminated critical residues of HCV E2 that were truncated or disordered in previous E2core structures, including the AS412 and VR2 regions (Figure 5A). While AS412 adopted two distinct conformations in E2ecto structures, the VR2 region consisted of a flexible loop that wraps around variable region 3 (VR3) (Figure 5A,E). In addition, the E2 ectodomain structures, although derived from different HCV strains, displayed a common disulfide bonding pattern, which was different from the disulfide pattern in E2 core structures (Figure 5B). For example, the E2 ectodomain structure revealed two disulfide bonds (Cys459–Cys486 and Cys581– Cys585) that were not found in previous E2core structures (Figure 5D,E). Cys459 and Cys486, which were disordered in the HEPC3-E2core$_{1a53}$ (Figure 2A) and AR3C-E2core$_{1a154}$ structures (Kong et al., 2013), form a disulfide bond that links the N- and C-termini of the VR2 loop (Figure 5B,D).

The E2 ectodomains in the new structures also included all potential N-linked glycosylation sites (PNGSs), offering the offering the opportunity to visualize potential interactions between E2 glycans and HCV bNAbs (Figure 5C). Glycan interactions with bNAbs are of interest since viral glycans are assembled by host-cell machinery and are therefore usually nonimmunogenic, thus neutralizing antibodies either avoid or evolve to accommodate carbohydrates on viral glycoproteins (Crispin et al., 2018). Both the HEPC3-E2ecto$_{1a53}$-HEPC46 and HEPC3-E2ecto$_{1b09}$ crystal structures show ordered glycan density at the Asn448 PNGS that contacts the HEPC3 CDRH1 (Figure 5F). Three HEPC3 CDRH1 residues that directly contact the Asn448 glycan are conserved between HEPC3, HEPC74, and AR3C (Figure 1A) and are encoded within the *V_H1–69* gene segment (Figure 7A), suggesting that some *V_H1–69*-encoded front layer-specific bNAbs are predisposed to recognize this Asn448 glycan. However, the different orientation of AR3C prevents its CDRH1 from interacting with the Asn448 glycan (Figure 3B). We also observed ordered density for the Asn430 glycan, which interacts with the HEPC3 V_L domain (Figure 5G).

The conserved AS412 region of E2 is a target of HCV vaccine efforts because it recognized by several bNAbs (Kong et al., 2015), but its conformation in the context of E2 had not been determined. Previous studies determined X-ray structures of synthetic peptides encompassing the AS412 antigenic site in complex with HCV bNAbs, revealing different conformations for AS412; for example, the AS412 peptide adopted a β-hairpin conformation when bound to the HCV1 and AP33 bNAbs (Kong et al., 2012a; Kong et al., 2012b; Potter et al., 2012) (Figure 6B) and an extended conformation when bound to the HC33.1 and 3/11 bNAbs (Li et al., 2015; Meola et al., 2015). The AS412 region also was investigated by electron microscopy using the AS412-specific bNAb HCV1, and the region was reported to be highly flexible in context of an E2 ectodomain lacking HVR1 (Kong et al., 2016), consistent with being disordered in the AR3C-E2core$_{1a154}$ crystal structure (Kong et al., 2013). Here we visualized the AS412 region conformation in both the HEPC3-

E2ecto$_{1b09}$ and HEPC3-E2ecto$_{1a53}$-HEPC46 structures (Figure 5A,6A). AS412 adopted a partially-open β-hairpin conformation in the HEPC3E2ecto$_{1b09}$ structure (Figure 5A), but adopted a different, more extended, conformation in the HEPC3-E2ecto$_{1a53}$-HEPC46 structure even though both complexes included HEPC3 (Figure 6A). When the residues in the AS412 regions determined in the context of E2 bound to HEPC3 Fab were aligned to the AS412 synthetic peptides from bNAb Fab-peptide structures, we found that AS412 adopts a multitude of conformations (Figure 6C). These results support the idea that AS412 is a flap-like structure that can adopt a variety of conformations, raising the question of whether the preferred conformation could be found in context of a targeted vaccine design.

Recognition of the E2 central β-sandwich by HEPC46

The E2core$_{1a53}$ and E2ecto$_{1a53}$ proteins were crystallized as ternarssy complexes with HEPC3 and the ß-sandwich-specific HEPC46 Fab. The binding of HEPC46 to E2ecto$_{1a53}$ did not change the structure of the E2 ectodomain (rmsd = 0.8 Å for superposition of 189 Cα atoms of E2ecto$_{1b09}$ and E2ecto$_{1a53}$) (Figure S4C). HEPC46 displayed a similar binding footprint in both E2 structures, sharing 14 contact residues in the central E2 β-sandwich, 2 residues in VR3, and 2 residues in the back layer (Figure S5 and Table S5). In the β-sandwich, 10 of 14 HEPC46 contact residues formed a linear epitope in the loop connecting two β-strands (residues 540–549) (Table S5). HEPC46 contacts the E2core predominantly with V_H domain residues, burying 727 Å^2 (80% of the total Fab BSA) in the HEPC46-E2core$_{1a53}$ structure and 674 Å^2 (83% of the total Fab BSA) in the HEPC46-E2ecto$_{1a53}$ structure (Table S5). The HEPC46 epitope lies in the proximal part of the ß-sandwich suggesting that HEPC46 is unlikely to prevent E2 from binding to the CD81 receptor, consistent with the poor neutralizing activity of this mAb (Bailey et al., 2017).

Germline precursors of front layer-specific HCV bNAbs

The HEPC3, HEPC74, and AR3C bNAbs exhibit different extents of somatic mutation from their common germline *V_H1–69* gene segment. HEPC3 and HEPC74 share 95% (HEPC3) and 92% (HEPC74) nucleotide identity with *V_H1–69* (Figure 1C). In contrast, AR3C has a higher rate of somatic mutations, sharing 86% nucleotide identity with *V_H1–69*. Since all three bNAbs are encoded by *V_H1–69*, their inferred germline sequences are the same within the V gene segment that encodes the CDRH1 and CDRH2 loops, with the exception of one substitution in framework region 3 of AR3C that results from being encoded by a different *V_H1–69* allele (*V_H1–69 *06* instead of *V_H1–69*01* for HEPC3 and HEPC74) (Figure 7A). Further sequence differences between the HEPC3rua, HEPC74rua, and AR3Crua sequences derive from two regions in CDRH3 flanking the shared R(K)-Y-C-G-G-G-X-C motif (Figure 7A).

To determine their breadths of recognition of different E2 proteins, we evaluated the binding of HEPC3, HEPC74, and AR3C IgGs to a panel of E2ecto proteins representing E2 envelopes from 19 genotype 1 strains. All front layer-specific bNAbs recognized 18 of 19 E2ecto envelopes; no detectable binding was found only for E2ecto from the 1a116 strain (Figure 7B). We also expressed HEPC3, HEPC74, and AR3C germline variants (HEPC3rua, HEPC74rua, and AR3Crua) and evaluated their binding to the panel of E2ecto variants. While HEPC3rua and AR3Crua recognized only 3 or 9 of the 19 variants, respectively,

HEPC74rua displayed broad- binding, recognizing 17 of 19 E2ecto variants (Figure 7B and Figure S6).

To evaluate the neutralization breadth of E2 front layer-specific bNAbs, we evaluated bNAbs in a neutralization assay using a panel of 19 genotype 1 HCVpp that represents 94% of the amino acid polymorphisms present at >5% frequency in a reference panel of 643 genotype 1 HCV isolates from GenBank. We defined the threshold for positive neutralization as a halfmaximal inhibitory concentration (IC_{50}) value of <10 μg/mL (Figure 7C). Mature HEPC3 and HEPC74 neutralized 18 of 19 (95%) HCV strains (Figure 7C; S7). The 1a116 strain, which was resistant to neutralization by HEPC3 and HEPC74, was weakly neutralized by AR3C. The germline precursors of HEPC3 and AR3C (HEPC3rua and AR3Crua) neutralized 2 of 19 (11%) or 7 of 19 (37%) strains, respectively (Figure 7C; S7). However, HEPC74rua displayed broad neutralizing activity, neutralizing 12 of 19 (63%) strains. Two HCV strains, 1a53 and 1a157, were bound and neutralized by all germline precursors (Figure 7C), suggesting that 1a53 and 1a157 ectodomains could be used to stimulate the development of lineage-specific potent bNAbs.

DISCUSSION

In this study, we structurally characterized two HCV E2 front layer-specific bNAbs (HEPC3 and HEPC74) previously isolated from individuals who spontaneously cleared HCV infection (Bailey et al., 2017) and a bNAb (AR3C) isolated from a person with chronic HCV infection (Law et al., 2008). These potent bNAbs predominantly use their V_H domains to recognize the conserved epitope in the front layer of E2 (Figure 2; Table S3–S4). We identified a common antibody lineage consisting of *VH1–69* antibodies sharing a common disulfide-linked motif in the CDRH3 loop that is partially encoded by a set of IGHD2 germline alleles (Figure 1A,B). The *V_H1–69* gene segment, represented at a high frequency in the human antibody repertoire, makes up a large portion of the HCV, HIV-1, and influenza-specific bNAbs described in the literature (Bailey et al., 2017; Pappas et al., 2014; Williams et al., 2015). In the case of HCV *V_H1–69*derived bNAbs, the IGHD2-encoded CDRH3 disulfide motif plays a critical role in the initial recognition of the E2 front layer by the germline precursors of HEPC3, HEPC74, and AR3C, as alanine or serine mutants of the cysteines showed nearly complete loss of binding and neutralization (Figure 4B). The CDRH3s of HEPC3 and AR3C are both long (19 and 20 residues, respectively), by comparison with an average length of 16 residues for the CDRH3s in human antibodies (Figure 1B) (Shi et al., 2014). The lengths of CDRH3 in HEPC3, HEPC74, and AR3C are probably restricted by the close proximity of the CD81 binding loop, which would likely clash with the tip of a longer CDRH3 loop, and by the formation of hydrogen bonds between the first cysteine in CDRH3 and Cys429 in the front layer of E2 (Figure 4C). Because mouse antibody CDRH3s are shorter than their human counterparts (Shi et al., 2014), and sequences including two cysteine residues are rare (Zemlin et al., 2003) in part due to the absence of D genes encoding cysteines in mice (Corbett et al., 1997), mouse models of HCV infection may not fully recapitulate human humoral neutralizing responses to HCV; in particular, E2 immunogens may fail to elicit HEPC3/HEPC74-like bNAbs in mice.

Antibody-antigen recognition can be described by induced-fit (Rosen et al., 2005) or lock-and-key models (Manivel et al., 2000). Structures of unliganded HEPC3, HEPC74, and AR3C Fabs showed that their CDRH3 loops adopt different orientations within their Fab combining sites despite presentation of a common disulfide motif (Figure 1D). Thus it might be expected that their CDRH3 loops would converge on a common conformation when bound to antigen through induced fit rearrangements, especially since the three bNAbs share a common *VH1–69* germline heavy chain origin and their germline CDRH1 and CDRH2 regions were therefore nearly or completely identical to each other (Figure 7A). Instead, we found that recognition of E2 antigens by these bNAbs was accomplished by pre-formed binding sites; i.e., a lock-and-key binding model (Figure 3, S3), which preserved a common interaction with antigen for their CDRH3 loops but resulted in different footprints for the CDRH1 and CDRH2 loops of the bNAbs with straight CDRH3s (HEPC3 and HEPC74) from the AR3C bNAb with a bent CDRH3 (Figure 3). Additional evidence that CDRH3 loop dictates the bNAb approach angle comes from subtle differences in the presentation of the straight disulfide motif in the unliganded HEPC3 and HEPC74 Fab structures (Figure 1D), which translate into slightly different E2binding orientations that each preserve the conserved interactions between the CDRH3 disulfide motif and the E2 front layer (Figure 3A). We hypothesize that the different conformations of the CDHR3s bearing a common disulfide motif in the three V_H*1–69*–encoded bNAbs dictate the preferential mode of engagement of bNAb germline precursors, overriding CDRH1 and CDRH2 interactions, and subsequent somatic mutations in those regions evolve to stabilize their distinct interactions and increase the bNAb affinity and breadth.

Multiple flexible loops and a relatively high degree of glycosylation make HCV E2 glycoproteins challenging targets to investigate with classical structural biological approaches (Castelli et al., 2014), thus previous E2 structures were limited to underglycosylated and truncated E2 cores (Khan et al., 2014; Kong et al., 2013). We adapted an approach used for RSV structural studies to co-transfect Fab and antigen genes (McLellan et al., 2013) in order to assemble stable E2-Fab complexes. This approach allowed us to determine structures of bNAb Fabs interacting with intact E2 ectodomains, revealing new information including the complete disulfide network of the E2 ectodomain (Figure 5B), glycan interactions with bNAbs (Figure 5B), and illuminating the previously-disordered AS412 and VR2 regions (Figure 5A,6A).

The AS412 region and the front layer of E2 are considered promising targets for rational immunogen design (Kong et al., 2015). These conserved regions of E2 have been reported to possess high structural flexibility (Kong et al., 2016), and attempts to stabilize these epitopes by rational design (Pierce et al., 2017) or transfer them onto heterologous protein scaffolds (He et al., 2015) have been made. AS412 was deleted or disordered in previous crystal structures of E2core (Khan et al., 2014; Kong et al., 2013) and adopted different conformations as a peptide complexed with different bNAbs (Figure 6B). Interestingly, in two E2 ectodomain structures, AS412 adopted two distinct conformations even when E2 was bound to a single bNAb, HEPC3 (Figure 6A). In contrast with the AS412 region, structures of HC84–1 and HC84–27 Fabs complexed with short peptides derived from the front layer E2 α1-helix showed that the peptides adopted the same conformation as the counterpart residues in the structure of the E2 core protein in complex with AR3C (Kong et

al., 2013; Krey et al., 2013). Taken together with the common conformation of the E2 front layer residues when presented in different formats, the finding that HEPC3 and AR3C, isolated from different individuals, utilize the common disulfide motif in the CDRH3 loop to recognize the epitope in the front layer of E2 adjacent to Cys429 – Cys503 disulfide bond (Figure 4C) suggests that this conserved region is relatively stable and accessible for antibody recognition. Therefore, the front layer of E2 remains a promising candidate for a targeted immunogen design.

Both HIV-1 and HCV are characterized by high mutation rates resulting in high antigenic variability (Yusim et al., 2010). Potent bNAbs against HIV-1 usually appear only after several years of infection and accumulation of a large number of somatic mutations (Mascola and Haynes, 2013; West et al., 2014), and their germline precursors rarely bind detectably to HIV-1 envelope glycoproteins (Xiao et al., 2009). In contrast, we found that HCV-specific bNAbs appeared early during the viral infection in two individuals who spontaneously cleared HCV infection (Bailey et al., 2017). In an accompanying article (Kinchen et al., 2018), we demonstrate that HEPC3 and HEPC74 played a direct role in spontaneous clearance of HCV infection in the human donors from whom they were isolated. This contrasts with HIV-1 infections, where viruses in individuals who produce bNAbs become resistant to those antibodies, and no documented cases of clearance of HIV-1 infection have yet been found (Klein et al., 2013; McCoy and Burton, 2017). Ongoing viral replication in the face of bNAbs, along with the latent HIV-1 reservoir of integrated proviruses, both represent barriers to HIV-1 cure. In contrast, there is no latent integrated form of HCV, and we found that most autologous viruses were sensitive to bNAbs HEPC3 and HEPC74. Acquisition of resistance to these bNAbs was accompanied by loss of viral replicative fitness, which was temporally associated with clearance of HCV infection. Neutralizing antibodies that clear a viral infection offer the rare opportunity to investigate the structural basis of recognition by effective broadly neutralizing antibodies. Thus our studies of HEPC3 and HEPC74 will facilitate immunogen design to elicit antibodies effective against multiple HCV variants and inform vaccine efforts against HIV-1 and other rapidly-mutating viruses.

The HCV bNAbs characterized here were not extensively somatically mutated (Figure 1C), suggesting that such antibodies could be stimulated with traditional vaccination strategies. In support of this idea, we found that germline precursors of potent bNAbs bind to several E2 ectodomains (Figure 7B). Furthermore, the broad binding and neutralization potencies of the HEPC74 germline precursor (Figure 7B,C) suggest that some $V_H1\text{–}69$-encoded bNAbs with the CDRH3 disulfide motif are naturally predisposed to recognize and neutralize diverse HCV strains. In addition, the identification of several E2 proteins that are recognized by the germline precursors of three $V_H1\text{–}69$-encoded bNAbs, HEPC3, HEPC74, and AR3C (Figure 7B), suggest that such immunogens could be used to stimulate the development of lineage-specific potent antibody response against HCV.

STAR METHODS

CONTACT FOR REAGENT AND RESOURCE SHARING

Further information and requests for resources and reagents should be directed to and will be fulfilled by Pamela J. Bjorkman (bjorkman@caltech.edu). The Bjorkman laboratory cannot lawfully distribute clones in the pTT5 vector. Those wishing to obtain these clones must first obtain a license from the National Research Council of Canada (see Key Resource Table).

METHODS DETAILS

IgG and Fab expression and purification.—Genes encoding the V_H and V_L domains of the HEPC3, HEPC74, HEPC46 (Bailey et al., 2017) and AR3C (Kong et al., 2013) bNAbs were synthesized as gBlocks gene fragments (IDT) and cloned into the pTT5-based vectors (NRC Biotechnology Research Institute). Reverted unmutated ancestor (rua) variants of HEPC3, HEPC74, and AR3C were inferred with IMGT/V-QUEST using complete sequences of heavy and light chain variable domains. IgGs and His- or Strep-tagged Fabs were produced in HEK293–6E cells by co-transfecting with appropriate heavy and light chain plasmids. HiTrap Protein A HP or HisTrap FF columns (GE Healthcare) were used to isolate IgGs or His-tagged Fabs from filtered culture supernatants followed by purification by size exclusion chromatography (SEC). Site-directed mutagenesis to replace two cysteines in the CDRH3s of HEPC3, HEPC74, and AR3C and their respective RUAs with either two alanines (2Cys→2Ala mutants) or two serines (2Cys→2Ser mutants) was performed using QuikChange Lightning SiteDirected Mutagenesis kit (Agilent).

Expression and purification of E2 constructs.—Genes encoding full-length 6x-His tagged HCV E2 ectodomains (E2ecto) (residues 384 – 643) for HCV strains 1a53 and 1b09 were cloned into the mammalian expression vector pHCMV3 that includes an N-terminal Ig-kappa secretion signal and expressed by transient transfection in HEK293–6E cells. For ELISA experiments, Histagged E2ecto proteins were purified from clarified supernatants using a HisTrap HP column (GE Healthcare) followed by SEC to separate monomeric E2ecto proteins from oligomeric species.

For structural studies, expression vectors encoding E2 ectodomains from strains 1a53 and 1b09 were constructed by removing the His-tag. E2core construct for 1a53 strain was engineered by removing HVR1 and E2 stem regions (residues 384–411 and 646–717), replacing VR2 (residues 460–485) with a Gly-Ser-Ser-Gly linker, and by making N448D and N576D mutations to remove the Asn448 and Asn576 potential N-linked glycosylation sites.

Expression and purification of E2-Fab complexes.—Complexes for structural studies were expressed by co-transfecting expression vectors encoding His- or Strep-tagged Fab(s) and untagged E2 and purifying Fab-E2 complexes from supernatants using His or Strep tag chromatography followed by SEC. HEK293–6E cells were grown in the presence of 5 μM kifunensine (Sigma) for expression of the HEPC3-E2core-HEPC46, HEPC3-E2ecto, and HEPC74-E2ecto complexes. Cells were grown in the absence of kifunensine to produce the HEPC3-E2ecto-HEPC46 complex.

Crystallization.—Commercially available screens (Hampton Research and Molecular Dimensions) were used to screen the initial crystallization conditions using vapor diffusion in sitting drops. HEPC3-Fab crystals were grown using 0.2 μL of protein (in TBS) and 0.2 μL of mother liquor (2.0 M ammonium sulfate, 0.3 M sodium chloride, and 0.1 M sodium cacodylate pH 6.3) and cryoprotected with Al's oil (Hampton Research). HEPC74-Fab crystals were grown using 0.2 μL of protein (in TBS) and 0.2 μL of mother liquor (0.2 M ammonium acetate, 0.1M BIS-Tris pH5.5, and 25% PEG 3,350) and cryoprotected with Fomblin® Y oil. AR3C-Fab crystals were grown using 0.2 μL of protein (in TBS) and 0.2 μL of mother liquor (0.2 M zinc acetate dihydrate pH 6.6, 11 % Sucrose, and 20% PEG 3,350) and cryoprotected in mother liquor supplemented with 15% (w/v) glycerol. HEPC46-Fab crystals were grown using 0.2 μL of protein (in TBS) and 0.2 μL of mother liquor (0.1 M Tris pH 8.0, 30% PEG 2,000) and cryoprotected with Fomblin® Y oil. HEPC3-E2core-HEPC46 crystals were grown using 0.2 μl of protein (in TBS) and 0.2 μl of mother liquor (0.02 M Nickel(II) chloride hexahydrate, 0.02 M magnesium chloride hexahydrate, 0.02 M cadmium chloride hydrate, 0.1 M sodium acetate trihydrate pH 4.5, 24% PEG 2,000) and cryoprotected in mother liquor supplemented with 20% (w/v) glycerol. HEPC3-E2ecto crystals were grown using 0.2 μL of protein (in TBS) and 0.2 μL of mother liquor (0.2M sodium bromide, 20% PEG 3,350) and cryoprotected using Al's oil. HEPC3-E2ecto-HEPC46 crystals were grown using 0.L μl of protein (in TBS) and 0.2 μL of mother liquor (0.2 M ammonium sulfate, 20% PEG 3,350) and cryoprotected in mother liquor supplemented with 20% (w/v) glycerol. All crystals were flash cooled in liquid nitrogen. HEPC74-E2ecto crystals were grown using 0.2 μL of protein (in TBS) and 0.2 μL of mother liquor (1% tryptone, 0.001 M sodium azide, 0.05 M HEPES sodium pH 7.0, 20% PEG 3,350) and cryoprotected using Al's oil.

Data collection and structure determinations.—X-ray diffraction data from cryopreserved crystals were collected at the Stanford Synchrotron Radiation Lightsource on beamline 12–2 using a PILATUS 6M detector (HEPC3-Fab, HEPC74-Fab, AR3C-Fab, HEPC46-Fab, and HEPC74-E2ecto), at the Advanced Photon Source on beamline 23-ID-D using a PILATUS3 6M detector (HEPC3-E2ecto and HEPC3-E2ecto-HEPC46), and at the Advanced Light Source on beamline 5.0.1 using a PILATUS3 6M detector (HEPC3-E2core-HEPC46). Images were processed and scaled using XDS (Kabsch, 2010), iMosflm (Battye et al., 2011), and Aimless as implemented in CCP4 software suite (Evans and Murshudov, 2013). Fab structures were solved by molecular replacement in Phaser (McCoy et al., 2007) using a model of AR3C (PDB 4MWF) or Fab 1281 (PDB 3P30). Fab-E2 complex structures were solved using molecular replacement using the separate molecules of HCV E2core (PDB 4MWF) and HEPC3, or HEPC3 and HEPC46, structures as search models. The models were refined and validated using Phenix.refine (Adams et al., 2010). Iterative manual model building and corrections were performed using Coot (Emsley and Cowtan, 2004). Glycans were initially interpreted and modeled using $F_o - F_c$ maps calculated with model phases contoured at 2σ, followed by $2F_o - F_c$ simulated annealing composite omit maps generated in Phenix in which modeled glycans were omitted to remove model bias (Adams et al., 2010). The quality of the final models was examined using MolProbity (Chen et al., 2010).

Models were superpositioned and figures rendered using the PyMOL molecular visualization system (Version 1.7, Schrödinger, LLC). The V_H/V_L domain orientation of HEPC3 on E2core relative to the AR3C was calculated using HIV Antibody Database software (West et al., 2013). Buried surface areas (BSAs) were determined using the PDBePISA web-based interactive tool (Krissinel and Henrick, 2007). Potential hydrogen bonds were assigned using criteria of a distance of <4.0 Å and an A-D-H angle of >90°, and the maximum distance allowed for a van der Waals interaction was 4.0 Å. Rmsd calculations were done in PyMOL following pairwise Cα alignments without excluding outliers.

ELISA binding analyses.—Soluble forms of full-length E2 ectodomains were coated overnight onto 96-well plates (Corning) at 1 μg/mL. Plates were blocked with 1% goat serum and 1% powdered milk in TBST buffer (TBS with 0.05% Tween-20) for 1 hr. Purified IgGs were assayed in duplicate at 4-fold serial dilutions, starting at 10 μg/mL IgGs bound to E2ecto proteins were detected using goat anti-human IgG horseradish peroxidase-conjugated secondary antibody (Southern Biotech, 1:4,000 dilution) and 1-Step Ultra TMB-ELISA substrate (Thermo Fisher Scientific) and reading the optical density read at 450 nm after stopping the reaction with 1M HCl. A non-linear regression analysis was performed on the resulting curves using Prism version 5 (GraphPad) to calculate EC_{50} values.

HCVpp production and neutralization assays.—HCVpp were produced by lipofectaminemediated transfection of HCV E1E2 and pNL4–3.Luc.R-E- plasmids into HEK293T cells as previously described (Hsu et al., 2003; Logvinoff et al., 2004). The panel of 19 heterologous genotype 1 HCVpp has been described previously (Bailey et al., 2015; Osburn et al., 2014). Neutralization assays were performed as described previously (Dowd et al., 2009). MAbs were serially diluted five-fold, starting at a concentration at 100 μg/ml and incubated with HCVpp for one hour prior to addition to Hep3B hepatoma cells. Luciferase activity was measured after three days and compared to that of HCVpp in media alone.

Supplementary Material

Refer to Web version on PubMed Central for supplementary material.

ACKNOWLEDGMENTS

We thank the Caltech Protein Expression Center for help with protein expression and Jens Kaiser, Christopher Barnes, Beth Stadtmueller, and Harry Gristick for training in crystallography. This research was supported by the National Institutes of Health grant R01 AI127469 (to J.R.B. and P.J.B.) (content is solely the responsibility of the authors and does not necessarily represent the official views of the NIH) and the Molecular Observatory at Caltech supported by the Gordon and Betty Moore Foundation. A.I.F. is a Cancer Research Institute Irvington Fellow supported by the Cancer Research Institute. This research used resources of the Advanced Photon Source, Advanced Light Source, and Stanford Synchrotron Radiation Lightsource, SLAC National Accelerator Laboratory. Use of the Advanced Photon Source was supported by the U.S.

Department of Energy, Office of Science, Office of Basic Energy Sciences, under Contract No. DE-AC02-06CH11357. The Advanced Light Source is a DOE Office of Science User Facility under contract no. DE-AC02-05CH11231. Use of the Stanford Synchrotron Radiation Lightsource, SLAC National Accelerator Laboratory, is supported by the U.S. Department of Energy, Office of Science, Office of Basic Energy Sciences under Contract No. DE-AC0276SF00515. The SSRL Structural Molecular Biology Program is supported by the DOE Office of Biological and Environmental Research and by NIHGMS P41GM103393.

REFERENCES

Adams PD, Afonine PV, Bunkoczi G, Chen VB, Davis IW, Echols N, Headd JJ, Hung LW, Kapral GJ, Grosse-Kunstleve RW, et al. (2010). PHENIX: a comprehensive Python-based system for macromolecular structure solution. Acta Crystallogr D Biol Crystallogr 66, 213–221. [PubMed: 20124702]

Bailey JR, Flyak AI, Cohen VJ, Li H, Wasilewski LN, Snider AE, Wang S, Learn GH, Kose N, Loerinc L, et al. (2017). Broadly neutralizing antibodies with few somatic mutations and hepatitis C virus clearance. JCI Insight 2.

Bailey JR, Wasilewski LN, Snider AE, El-Diwany R, Osburn WO, Keck Z, Foung SK, and Ray SC (2015). Naturally selected hepatitis C virus polymorphisms confer broad neutralizing antibody resistance. J Clin Invest 125, 437–447. [PubMed: 25500884]

Battye TG, Kontogiannis L, Johnson O, Powell HR, and Leslie AG (2011). iMOSFLM: a new graphical interface for diffraction-image processing with MOSFLM. Acta Crystallogr D Biol Crystallogr 67, 271–281. [PubMed: 21460445]

Castelli M, Clementi N, Sautto GA, Pfaff J, Kahle KM, Barnes T, Doranz BJ, Dal Peraro M, Clementi M, Burioni R, et al. (2014). HCV E2 core structures and mAbs: something is still missing. Drug Discov Today 19, 1964–1970. [PubMed: 25172800]

Chen VB, Arendall WB, 3rd, Headd JJ, Keedy DA, Immormino RM, Kapral GJ, Murray LW, Richardson JS, and Richardson DC (2010). MolProbity: all-atom structure validation for macromolecular crystallography. Acta Crystallogr D Biol Crystallogr 66, 12–21. [PubMed: 20057044]

Corbett SJ, Tomlinson IM, Sonnhammer EL, Buck D, and Winter G (1997). Sequence of the human immunoglobulin diversity (D) segment locus: a systematic analysis provides no evidence for the use of DIR segments, inverted D segments, “minor” D segments or D-D recombination. J Mol Biol 270, 587–597. [PubMed: 9245589]

Crispin M, Ward AB, and Wilson IA (2018). Structure and Immune Recognition of the HIV Glycan Shield. Annu Rev Biophys

Deng L, Zhong L, Struble E, Duan H, Ma L, Harman C, Yan H, Virata-Theimer ML, Zhao Z, Feinstone S, et al. (2013). Structural evidence for a bifurcated mode of action in the antibody-mediated neutralization of hepatitis C virus. Proc Natl Acad Sci U S A 110, 7418–7422. [PubMed: 23589879]

Denniston MM, Klevens RM, McQuillan GM, and Jiles RB (2012). Awareness of infection, knowledge of hepatitis C, and medical follow-up among individuals testing positive for hepatitis C: National Health and Nutrition Examination Survey 2001–2008. Hepatology 55, 1652–1661. [PubMed: 22213025]

Dowd KA, Netski DM, Wang XH, Cox AL, and Ray SC (2009). Selection Pressure from Neutralizing Antibodies Drives Sequence Evolution during Acute Infection with Hepatitis C Virus. Gastroenterology 136, 2377–2386. [PubMed: 19303013]

Emsley P, and Cowtan K (2004). Coot: model-building tools for molecular graphics. Acta Crystallogr D Biol Crystallogr 60, 2126–2132. [PubMed: 15572765]

Evans PR, and Murshudov GN (2013). How good are my data and what is the resolution? Acta Crystallogr D Biol Crystallogr 69, 1204–1214. [PubMed: 23793146]

Freedman H, Logan MR, Law JL, and Houghton M (2016). Structure and Function of the Hepatitis C Virus Envelope Glycoproteins E1 and E2: Antiviral and Vaccine Targets. ACS Infect Dis 2, 749–762. [PubMed: 27933781]

Giang E, Dorner M, Prentoe JC, Dreux M, Evans MJ, Bukh J, Rice CM, Ploss A, Burton DR, and Law M (2012). Human broadly neutralizing antibodies to the envelope glycoprotein complex of hepatitis C virus. Proc Natl Acad Sci U S A 109, 6205–6210. [PubMed: 22492964]

Gopal R, Jackson K, Tzarum N, Kong L, Ettenger A, Guest J, Pfaff JM, Barnes T, Honda A, Giang E, et al. (2017). Probing the antigenicity of hepatitis C virus envelope glycoprotein complex by high-throughput mutagenesis. PLoS Pathog 13, e1006735. [PubMed: 29253863]

He L, Cheng Y, Kong L, Azadnia P, Giang E, Kim J, Wood MR, Wilson IA, Law M, and Zhu J (2015). Approaching rational epitope vaccine design for hepatitis C virus with meta-server and multivalent scaffolding. Sci Rep 5, 12501. [PubMed: 26238798]

Hsu M, Zhang J, Flint M, Logvinoff C, Cheng-Mayer C, Rice CM, and McKeating JA (2003). Hepatitis C virus glycoproteins mediate pH-dependent cell entry of pseudotyped retroviral particles. Proc Natl Acad Sci U S A 100, 7271–7276. [PubMed: 12761383]

Kabsch W (2010). Integration, scaling, space-group assignment and post-refinement. Acta Crystallogr D Biol Crystallogr 66, 133–144. [PubMed: 20124693]

Khan AG, Miller MT, and Marcotrigiano J (2015). HCV glycoprotein structures: what to expect from the unexpected. Curr Opin Virol 12, 53–58. [PubMed: 25790756]

Khan AG, Whidby J, Miller MT, Scarborough H, Zatorski AV, Cygan A, Price AA, Yost SA, Bohannon CD, Jacob J, et al. (2014). Structure of the core ectodomain of the hepatitis C virus envelope glycoprotein 2. Nature 509, 381–384. [PubMed: 24553139]

Kinchen VJ, Zahid M, Flyak AI, Soliman M, Doranz B, Ray SC, Cox AL, Crowe JE, Bjorkman PJ, Shaw GM, et al. (2018). Broadly neutralizing antibody mediated clearance of human Hepatitis C virus infection. Submitted for review

Klein F, Mouquet H, Dosenovic P, Scheid JF, Scharf L, and Nussenzweig MC (2013). Antibodies in HIV-1 vaccine development and therapy. Science 341, 1199–1204. [PubMed: 24031012]

Kong L, Giang E, Nieusma T, Kadam RU, Cogburn KE, Hua Y, Dai X, Stanfield RL, Burton DR, Ward AB, et al. (2013). Hepatitis C virus E2 envelope glycoprotein core structure. Science 342, 1090–1094. [PubMed: 24288331]

Kong L, Giang E, Nieusma T, Robbins JB, Deller MC, Stanfield RL, Wilson IA, and Law M (2012a). Structure of hepatitis C virus envelope glycoprotein E2 antigenic site 412 to 423 in complex with antibody AP33. J Virol 86, 13085–13088. [PubMed: 22973046]

Kong L, Giang E, Robbins JB, Stanfield RL, Burton DR, Wilson IA, and Law M (2012b). Structural basis of hepatitis C virus neutralization by broadly neutralizing antibody HCV1. Proc Natl Acad Sci U S A 109, 9499–9504. [PubMed: 22623528]

Kong L, Jackson KN, Wilson IA, and Law M (2015). Capitalizing on knowledge of hepatitis C virus neutralizing epitopes for rational vaccine design. Curr Opin Virol 11, 148–157. [PubMed: 25932568]

Kong L, Lee DE, Kadam RU, Liu T, Giang E, Nieusma T, Garces F, Tzarum N, Woods VL, Jr., Ward AB, et al. (2016). Structural flexibility at a major conserved antibody target on hepatitis C virus E2 antigen. Proc Natl Acad Sci U S A

Krey T, Meola A, Keck ZY, Damier-Piolle L, Foung SK, and Rey FA (2013). Structural basis of HCV neutralization by human monoclonal antibodies resistant to viral neutralization escape. PLoS Pathog 9, e1003364. [PubMed: 23696737]

Krissinel E, and Henrick K (2007). Inference of macromolecular assemblies from crystalline state. J Mol Biol 372, 774–797. [PubMed: 17681537]

Law M, Maruyama T, Lewis J, Giang E, Tarr AW, Stamataki Z, Gastaminza P, Chisari FV, Jones IM, Fox RI, et al. (2008). Broadly neutralizing antibodies protect against hepatitis C virus quasispecies challenge. Nat Med 14, 25–27. [PubMed: 18064037]

Li Y, Pierce BG, Wang Q, Keck ZY, Fuerst TR, Foung SK, and Mariuzza RA (2015). Structural basis for penetration of the glycan shield of hepatitis C virus E2 glycoprotein by a broadly neutralizing human antibody. J Biol Chem 290, 10117–10125. [PubMed: 25737449]

Logvinoff C, Major ME, Oldach D, Heyward S, Talal A, Balfe P, Feinstone SM, Alter H, Rice CM, and McKeating JA (2004). Neutralizing antibody response during acute and chronic hepatitis C virus infection. Proc Natl Acad Sci U S A 101, 10149–10154. [PubMed: 15220475]

Manivel V, Sahoo NC, Salunke DM, and Rao KV (2000). Maturation of an antibody response is governed by modulations in flexibility of the antigen-combining site. Immunity 13, 611–620. [PubMed: 11114374]

Mascola JR, and Haynes BF (2013). HIV-1 neutralizing antibodies: understanding nature's pathways. Immunol Rev 254, 225–244. [PubMed: 23772623]

McCoy AJ, Grosse-Kunstleve RW, Adams PD, Winn MD, Storoni LC, and Read RJ (2007). Phaser crystallographic software. J Appl Crystallogr 40, 658–674. [PubMed: 19461840]

McCoy LE, and Burton DR (2017). Identification and specificity of broadly neutralizing antibodies against HIV. Immunol Rev 275, 11–20. [PubMed: 28133814]

McLellan JS, Chen M, Leung S, Graepel KW, Du X, Yang Y, Zhou T, Baxa U, Yasuda E, Beaumont T, et al. (2013). Structure of RSV fusion glycoprotein trimer bound to a prefusion-specific neutralizing antibody. Science 340, 1113–1117. [PubMed: 23618766]

Meola A, Tarr AW, England P, Meredith LW, McClure CP, Foung SK, McKeating JA, Ball JK, Rey FA, and Krey T (2015). Structural flexibility of a conserved antigenic region in hepatitis C virus glycoprotein E2 recognized by broadly neutralizing antibodies. J Virol 89, 2170–2181. [PubMed: 25473061]

Meunier JC, Russell RS, Goossens V, Priem S, Walter H, Depla E, Union A, Faulk KN, Bukh J, Emerson SU, et al. (2008). Isolation and characterization of broadly neutralizing human monoclonal antibodies to the e1 glycoprotein of hepatitis C virus. J Virol 82, 966–973. [PubMed: 17977972]

Micallef JM, Kaldor JM, and Dore GJ (2006). Spontaneous viral clearance following acute hepatitis C infection: a systematic review of longitudinal studies. J Viral Hepat 13, 34–41. [PubMed: 16364080]

Osburn WO, Snider AE, Wells BL, Latanich R, Bailey JR, Thomas DL, Cox AL, and Ray SC (2014). Clearance of hepatitis C infection is associated with the early appearance of broad neutralizing antibody responses. Hepatology 59, 2140–2151. [PubMed: 24425349]

Pappas L, Foglierini M, Piccoli L, Kallewaard NL, Turrini F, Silacci C, FernandezRodriguez B, Agatic G, Giacchetto-Sasselli I, Pellicciotta G, et al. (2014). Rapid development of broadly influenza neutralizing antibodies through redundant mutations. Nature 516, 418–422. [PubMed: 25296253]

Pestka JM, Zeisel MB, Blaser E, Schurmann P, Bartosch B, Cosset FL, Patel AH, Meisel H, Baumert J, Viazov S, et al. (2007). Rapid induction of virus-neutralizing antibodies and viral clearance in a single-source outbreak of hepatitis C. Proc Natl Acad Sci U S A 104, 6025–6030. [PubMed: 17392433]

Pierce BG, Boucher EN, Piepenbrink KH, Ejemel M, Rapp CA, Thomas WD, Jr., Sundberg EJ, Weng Z, and Wang Y (2017). Structure-Based Design of Hepatitis C Virus Vaccines That Elicit Neutralizing Antibody Responses to a Conserved Epitope. J Virol 91.

Potter JA, Owsianka AM, Jeffery N, Matthews DJ, Keck ZY, Lau P, Foung SK, Taylor GL, and Patel AH (2012). Toward a hepatitis C virus vaccine: the structural basis of hepatitis C virus neutralization by AP33, a broadly neutralizing antibody. J Virol 86, 1292312932.

Rosen HR (2017). “Hep C, where art thou”: What are the remaining (fundable) questions in hepatitis C virus research? Hepatology 65, 341–349. [PubMed: 27640881]

Rosen O, Chill J, Sharon M, Kessler N, Mester B, Zolla-Pazner S, and Anglister J (2005). Induced fit in HIV-neutralizing antibody complexes: evidence for alternative conformations of the gp120 V3 loop and the molecular basis for broad neutralization. Biochemistry 44, 7250–7258. [PubMed: 15882063]

Shi B, Ma L, He X, Wang X, Wang P, Zhou L, and Yao X (2014). Comparative analysis of human and mouse immunoglobulin variable heavy regions from IMGT/LIGM-DB with IMGT/HighV-QUEST. Theor Biol Med Model 11, 30. [PubMed: 24992938]

West AP, Jr., Scharf L, Horwitz J, Klein F, Nussenzweig MC, and Bjorkman PJ (2013). Computational analysis of anti-HIV-1 antibody neutralization panel data to identify potential functional epitope residues. Proc Natl Acad Sci U S A 110, 10598–10603. [PubMed: 23754383]

West AP, Scharf L, Scheid JF, Klein F, Bjorkman PJ, and Nussenzweig MC (2014). Structural Insights on the Role of Antibodies in HIV-1 Vaccine and Therapy. Cell 156, 633–648. [PubMed: 24529371]

Williams WB, Liao HX, Moody MA, Kepler TB, Alam SM, Gao F, Wiehe K, Trama AM, Jones K, Zhang R, et al. (2015). HIV-1 VACCINES. Diversion of HIV-1 vaccine-induced immunity by gp41-microbiota cross-reactive antibodies. Science 349, aab1253.

Xiao X, Chen W, Feng Y, Zhu Z, Prabakaran P, Wang Y, Zhang MY, Longo NS, and Dimitrov DS (2009). Germline-like predecessors of broadly neutralizing antibodies lack measurable binding to HIV-1 envelope glycoproteins: implications for evasion of immune responses and design of vaccine immunogens. Biochem Biophys Res Commun 390, 404–409. [PubMed: 19748484]

Yusim K, Fischer W, Yoon H, Thurmond J, Fenimore PW, Lauer G, Korber B, and Kuiken C (2010). Genotype 1 and global hepatitis C T-cell vaccines designed to optimize coverage of genetic diversity. J Gen Virol 91, 1194–1206. [PubMed: 20053820]

Zeisel MB, Fofana I, Fafi-Kremer S, and Baumert TF (2011). Hepatitis C virus entry into hepatocytes: molecular mechanisms and targets for antiviral therapies. J Hepatol 54, 566–576. [PubMed: 21146244]

Zemlin M, Klinger M, Link J, Zemlin C, Bauer K, Engler JA, Schroeder HW, Jr., and Kirkham PM (2003). Expressed murine and human CDR-H3 intervals of equal length exhibit distinct repertoires that differ in their amino acid composition and predicted range of structures. J Mol Biol 334, 733–749. [PubMed: 14636599]

Zibbell JE, Asher AK, Patel RC, Kupronis B, Iqbal K, Ward JW, and Holtzman D (2018). Increases in Acute Hepatitis C Virus Infection Related to a Growing Opioid Epidemic and Associated Injection Drug Use, United States, 2004 to 2014. Am J Public Health 108, 175181.

HIGHLIGHTS

- HCV E2-targeting bNAbs HEPC3/HEPC74 were isolated from individuals who cleared infection
- Structures of HEPC3/HEPC74 in complex with E2 ectodomain reveal new binding orientation
- Germline-encoded CDRH3 motif plays a critical role in initial E2 recognition
- Several natural E2 variants bind to HEPC3/HEPC74-like germline precursors

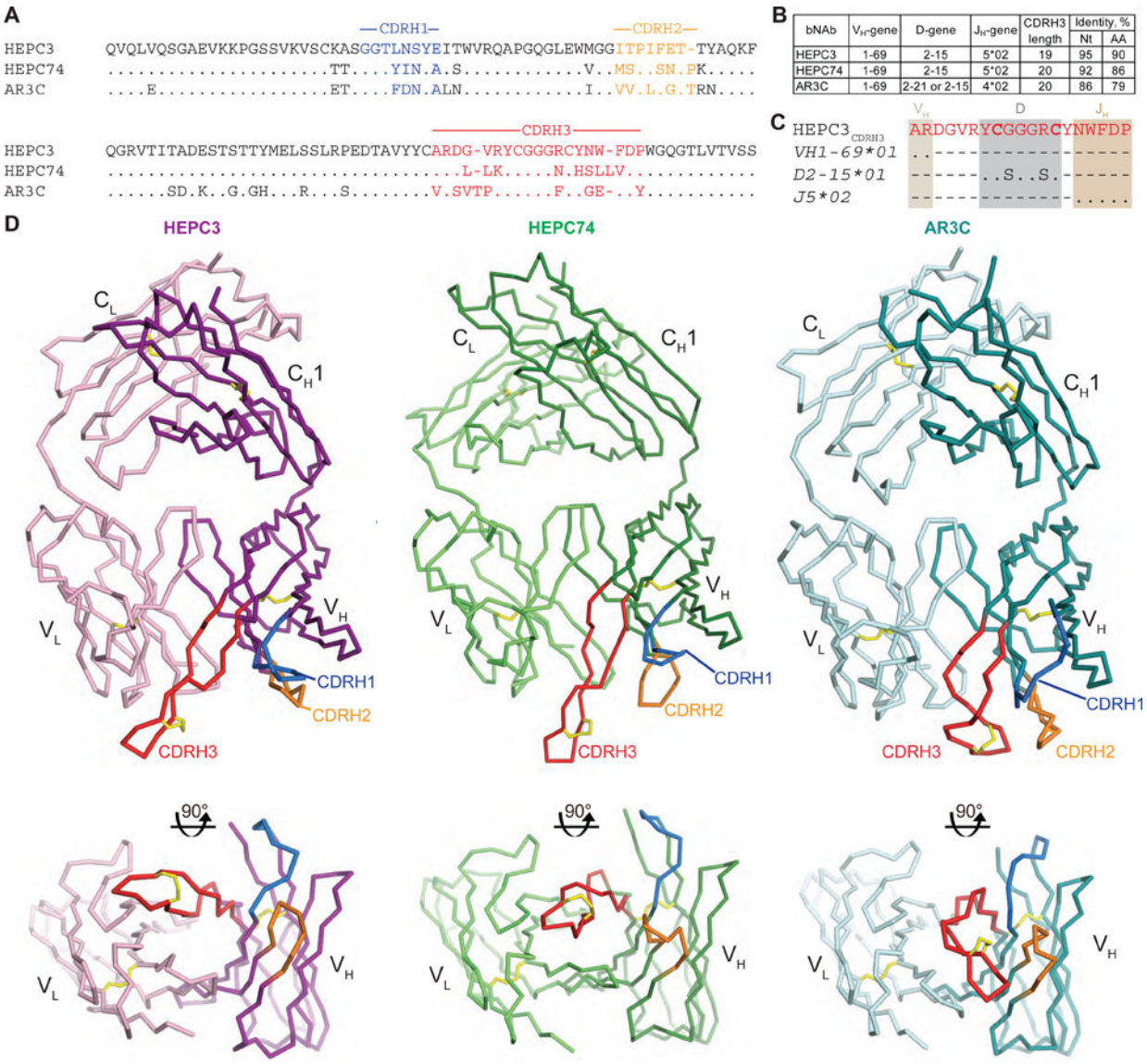

Figure 1. The shared CDRH3 motif in E2 front layer-specific bNAbs adopts different orientations.

(A) Sequence alignment of the recombined antibody heavy chain (top) and light chain (bottom) variable gene sequences of HEPC3, HEPC74, and AR3C. CDR loops were defined based on IMGT nomenclature and colored blue (CDRH1), orange (CDRH2), and red (CDRH3). Dots indicate identical amino acids; dashes indicate gaps. (B) V_H, D, and J_H gene usage for HEPC3, HEPC74, and AR3C. (C) Sequence alignment of CDRH3s from mature HEPC3 and HEPC3 germline precursor genes determined by IMGT/V-QUEST. Dots indicated identical amino acids and dashes indicate regions encoded by other gene segments or Nnucleotide additions. Two cysteines encoded by the D gene segment are highlighted in bold. (D) Side (top) and top (bottom) views of Fab structures of HEPC3, HEPC74, and AR3C. The crystal structures were superimposed on their V_H and V_L domains. Protein backbones are shown as ribbons and CDR loops are blue (CDRH1), orange (CDRH2), and red (CDRH3). Disulfide bonds are shown as yellow sticks. See also Figure S2, Table S1.

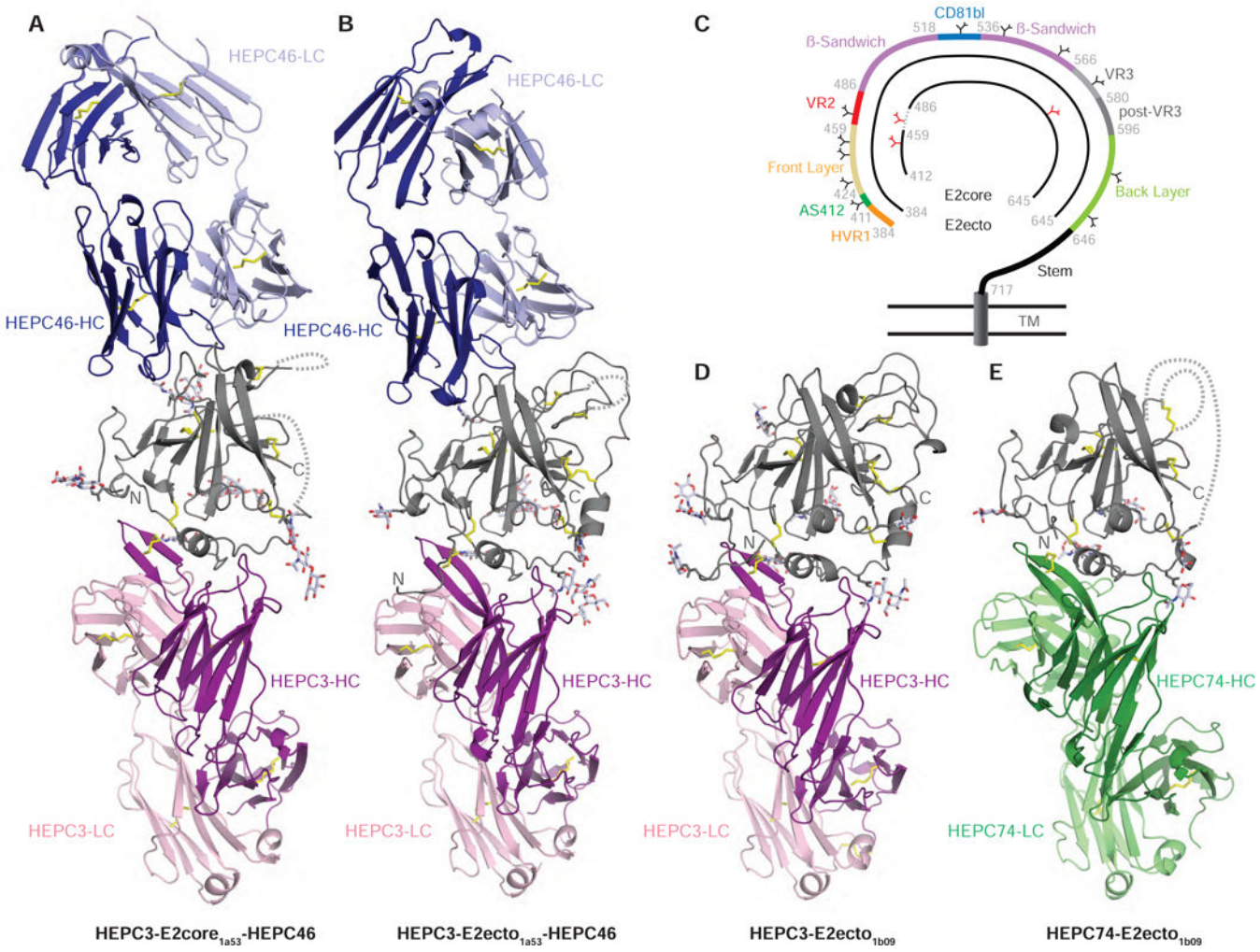

Figure 2. HEPC3 and HEPC74 recognize E2ecto similarly.

The crystal structure of HEPC3E2core$_{1a53}$-HEPC46 (A), HEPC3-E2ecto$_{1a53}$-HEPC46 (B), HEPC3-E2ecto$_{1b09}$ (D), and HEPC74E2ecto$_{1b09}$ (E) complexes are displayed as cartoon representations. E2 – grey, HEPC3-HC – purple, HEPC3-LC – pink, HEPC74-HC – dark green, HEPC74-LC – light green, HEPC46-HC – dark blue, HEPC46-LC – light blue. Disulfide bonds are shown as yellow sticks and E2 glycans are shown as sticks with light blue, red, and dark blue colors for carbon, oxygen, and nitrogen atoms, respectively. Dashed lines indicated disordered regions. (C) E2 regions included in E2core and E2ecto structures. E2 regions are colored by structural components: HVR1 (orange), AS412 (dark green), front layer (yellow), VR2 (red), β-sandwich (violet), CD81bl (blue), VR3 (light grey), post-VR3 (dark grey), back layer (green), and stem (black). Dashed line indicates the G-S-S-G linker, deleted glycosylation sites in E2 core construct are highlighted in red. See also Figure S1, S5, Table S2–S5.

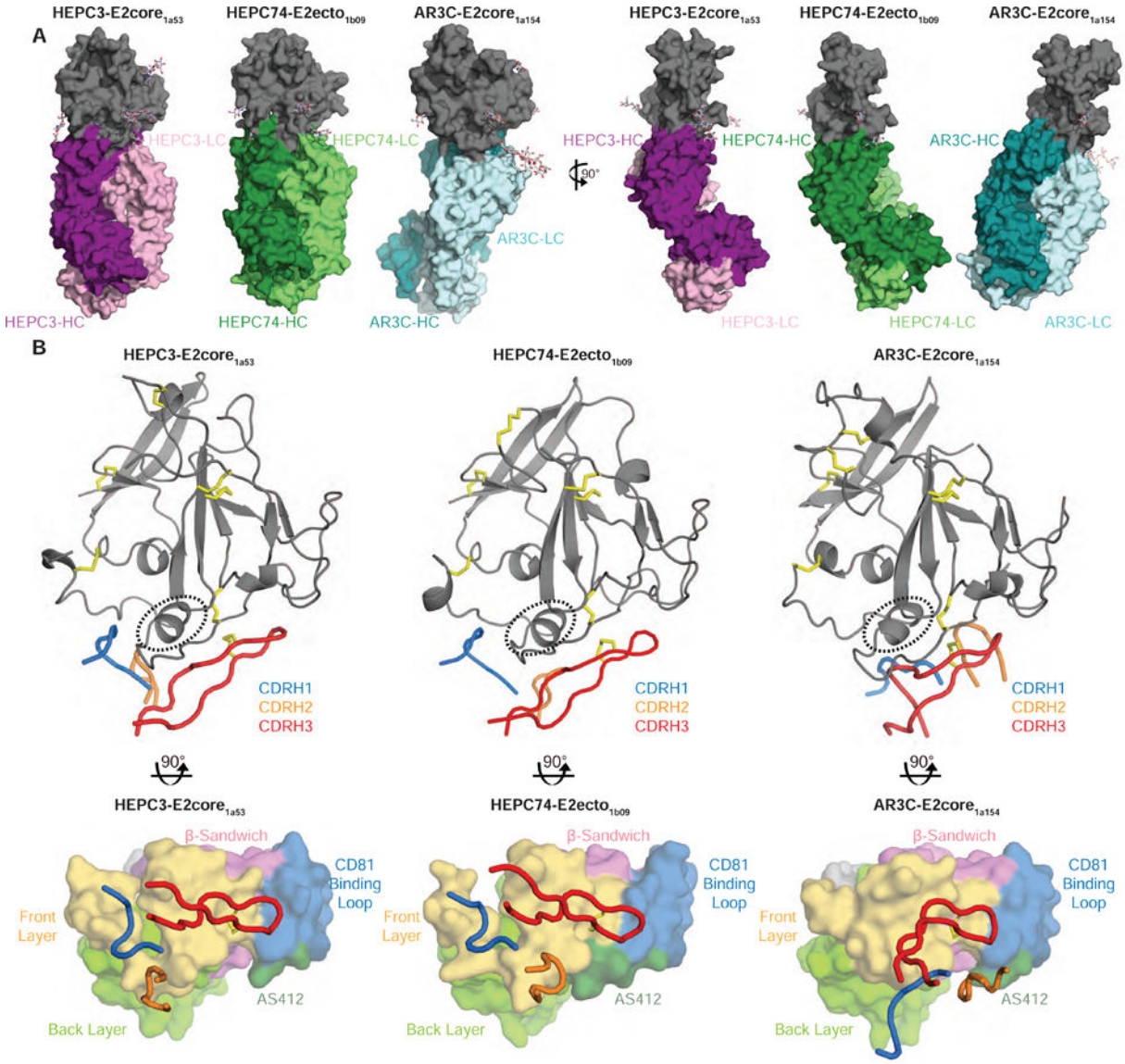

Figure 3. HEPC3 and HEPC74 recognize HCV E2 using a disulfide-linked CDRH3 motif.

(A) Surface representations of the HEPC3-E2core$_{1a53}$-HEPC46, HEPC74-E2ecto$_{1b09}$, and AR3CE2core$_{1a154}$ (PDB 4MWF) (Kong et al., 2013) structures. The HEPC46 Fab is not shown for clarity. E2 glycans are shown as sticks with light blue, red, blue colors for carbon, oxygen, and nitrogen atoms, respectively. E2cores – grey, HEPC3-HC – purple, HEPC3-LC – pink, HEPC74HC – dark green, HEPC74-LC – light green, AR3C-HC – cyan, AR3C-LC – light cyan. (B) Comparison of the heavy chain CDR (CDRH) loop positions in E2 core complex structures with HEPC3, HEPC74, and AR3C. E2core structures are shown as cartoon representation (top) and as surface representation (bottom). CDRH loops are blue (CDRH1), orange (CDRH2), and red (CDRH3) tubes. Disulfide bonds and the α1-helix are shown as yellow sticks and dashed ovals, respectively, in the top images. E2 surfaces in the bottom images are colored by structural components: AS412 (dark green), front layer (yellow), VR2 (red), β-sandwich (violet), CD81bl (blue), VR3 (light grey), post-VR3 (dark grey), back layer (light green). See also Figure S3.

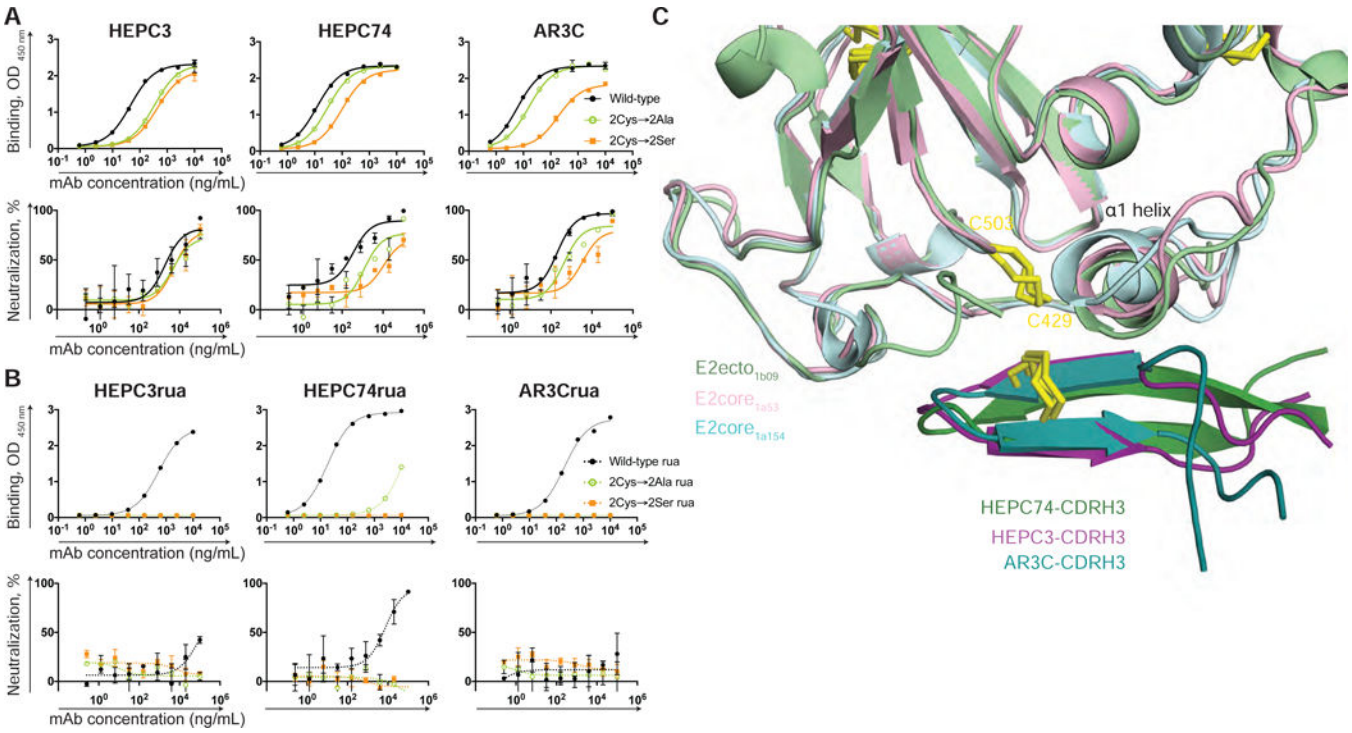

Figure 4. The intra-CDRH3 disulfide bond in E2 front layer-specific bNAbs is required for maximal binding and neutralization.

(A) Binding to E2ecto$_{1a53}$ (top) and neutralizing activity against 1a53 strain HCVpp (bottom) of wild-type bNAbs (black) and corresponding CDRH3 2Cys→2Ala (green) or CDRH3 2Cys→2Ser (orange) double mutants. Means ± s.d. of duplicates are shown. One experiment representative of two independent experiments is shown. (B) Binding to E2ecto$_{1a53}$ (top) and neutralizing activity against 1a53 strain HCVpp (bottom) of inferred germline precursors HEPC3rua, HEPC74rua, and AR3Crua (black) and corresponding CDRH3 2Cys→2Ala (green) and CDRH3 2Cys→2Ser (orange) double mutants. One experiment representative of two independent experiments is shown. Means ± s.d. of duplicates are shown. (C) Superposition of HEPC3-E2ecto$_{1b09}$ (light green), HEPC3-E2core$_{1a53}$ (pink), and AR3CE2core$_{1a154}$ (light cyan) structures. Structures were superimposed on the E2cores and are shown as cartoon representations with CDRH3 loops in green (HEPC74), purple (HEPC3), and cyan (AR3C). Disulfide bonds are shown as yellow sticks.

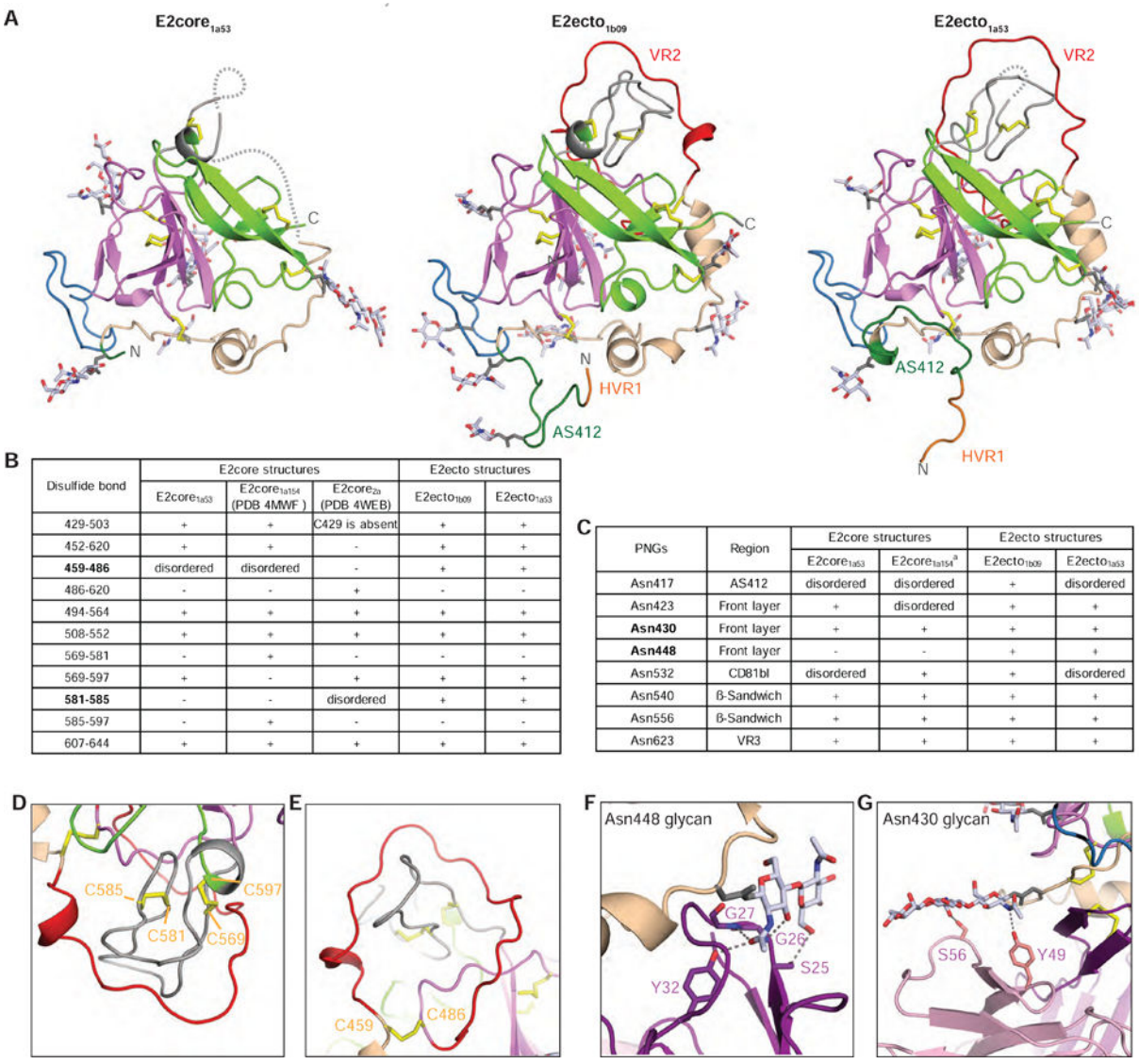

B

Disulfide bond	E2core structures			E2ecto structures	
	$E2core_{1a53}$	$E2core_{1a154}$ (PDB 4MWF)	$E2core_{2a}$ (PDB 4WEB)	$E2ecto_{1b09}$	$E2ecto_{1a53}$
429-503	+	+	C429 is absent	+	+
452-620	+	+	-	+	+
459-486	disordered	disordered	-	+	+
486-620	-	-	+	-	-
494-564	+	+	+	+	+
508-552	+	+	+	+	+
569-581	-	+	-	-	-
569-597	+	-	+	+	+
581-585	-	-	disordered	+	+
585-597	-	+	-	-	-
607-644	+	+	+	+	+

C

PNGs	Region	E2core structures		E2ecto structures	
		$E2core_{1a53}$	$E2core_{1a154}$[a]	$E2ecto_{1b09}$	$E2ecto_{1a53}$
Asn417	AS412	disordered	disordered	+	disordered
Asn423	Front layer	+	disordered	+	+
Asn430	Front layer	+	+	+	+
Asn448	Front layer	-	-	+	+
Asn532	CD81bl	disordered	+	+	disordered
Asn540	ß-Sandwich	+	+	+	+
Asn556	ß-Sandwich	+	+	+	+
Asn623	VR3	+	+	+	+

Figure 5. Soluble E2 ectodomain structures reveal conformations of disordered or truncated regions of E2core.

(A) Structures of HEPC3-$E2core_{1a53}$-HEPC46, HEPC3-$E2ecto_{1b09}$, and HEPC3-$E2core_{1a53}$-HEPC46 complexes displayed as cartoon representations (HVR1 (orange), AS412 (dark green), front layer (yellow), VR2 (red), ß-sandwich (violet), CD81bl (blue), VR3 (light grey), post-VR3 (dark grey), and back layer (green)) with regions of E2 that were truncated or disordered in E2core structures indicated. Disulfide bonds are yellow sticks; E2core glycans are sticks with light blue, red, blue colors for carbon, oxygen, and nitrogen atoms, respectively. Dashed lines indicate disordered regions. (B) Observed disulfide bonds in E2core and E2ecto structures. Disulfide bonds visible only in E2ecto structures are highlighted in bold. (C) Ordered glycans in E2core and E2ecto structures. Glycans that contact HEPC3 are highlighted in bold. (D) Close proximity of Cys581-Cys585 and Cys569-Cys597 disulfide bonds ($E2ecto_{1b09}$ structure). In the $E2core_{1a154}$ structure (Kong et al., 2013), the disulfide pattern is: Cys561–Cys581 and Cys585–Cys597. (E) Structure of the VR2 loop ($E2ecto_{1b09}$ structure) (red). The Cys459-Cys486 disulfide bond that is disordered

in the E2 core structures is shown. In the $E2core_{2a}$ structure (Khan et al., 2014), Cys486 disulfide bonds with Cys620, likely due to deletion of the portion of E2 that includes Cys452, the Cys620 partner. (F) CDRH1 interactions with Asn448 glycan with interacting residues shown as sticks. Potential H-bonds are shown as black dashed lines, and residues at the interface are indicated. (G) HEPC3 light chain interactions with Asn430 glycan with interacting residues shown as sticks. Potential H-bonds are shown as black dashed lines, and residues at the interface are indicated. See also Figure S4.

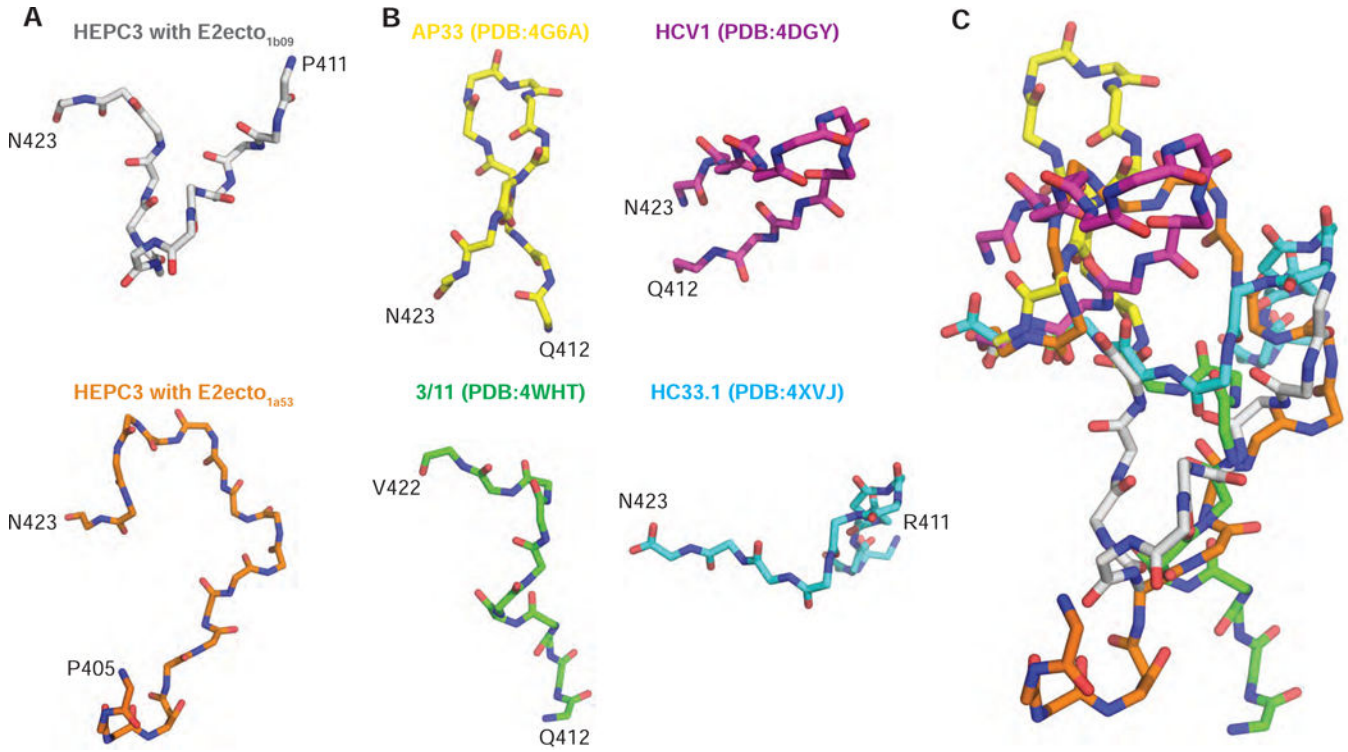

Figure 6. The AS412 region can adopt multiple conformations.

(A) Structures of the N-terminal portion of E2ecto including the AS412 region for the HEPC3-E2ecto1b09 and HEPC3E2ecto1a53-HEPC46 complexes. (B) Structures of AS412 peptides in complex with the indicated bNAbs. Only backbone atoms are shown. N- and C-termini are labeled. (C) Superposition of AS412 structures from (A) and (B). Structures were aligned on the C-termini.

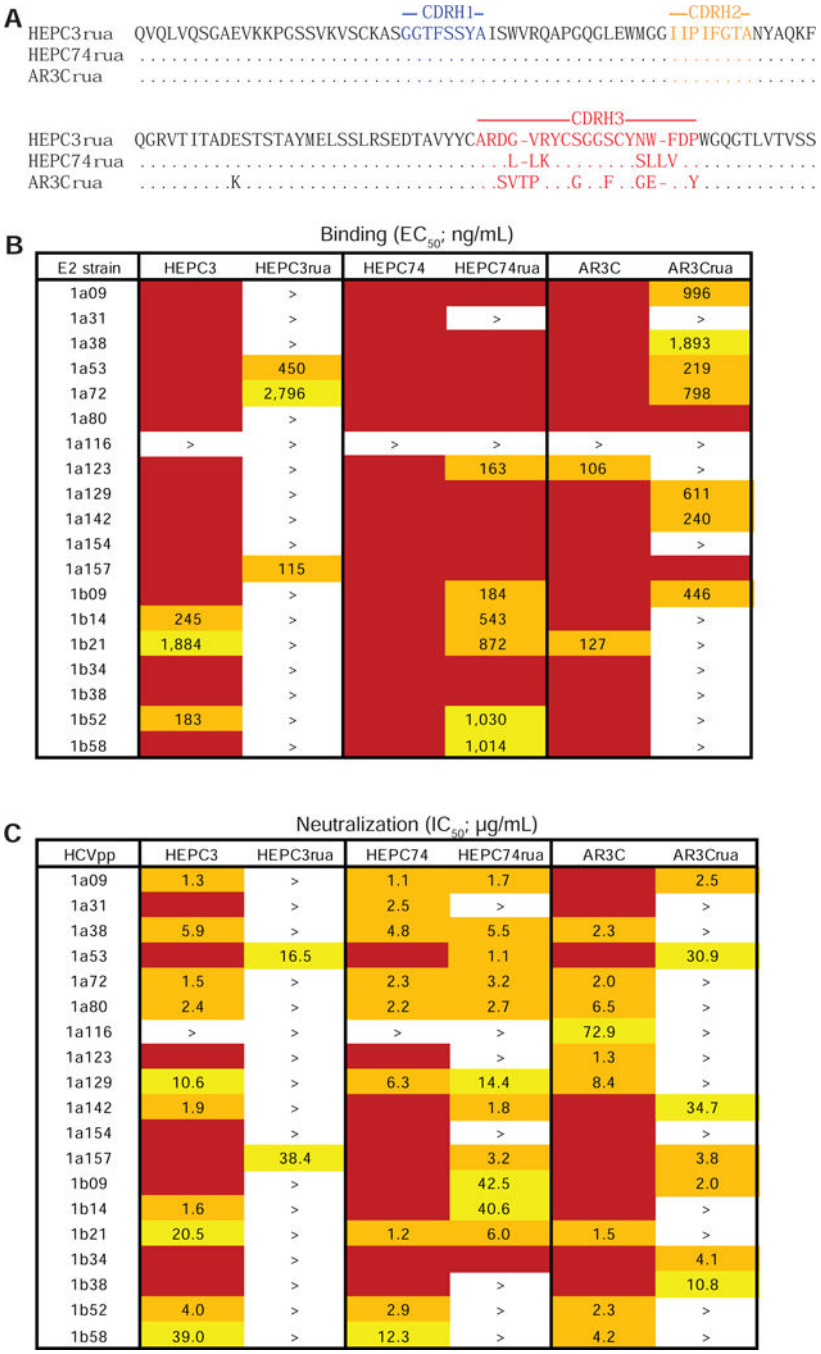

Figure 7. Germline precursors of E2 front layer-specific bNAbs neutralize diverse HCV strains.

(A) Sequence alignment of antibody heavy chain variable domains of the inferred germline precursors HEPC3rua, HEPC74rua, and AR3Crua. CDRs were defined based on IMGT nomenclature and colored blue (CDRH1), orange (CDRH2), and red (CDRH3). Dots indicate identical amino acids and dashes indicate gaps. (B) Heat map showing the binding of HEPC3, HEPC74, AR3C and their germline precursors to a panel of HCV genotype 1 E2ecto proteins. The EC_{50} value for each E2ecto-mAb combination is shown, with dark red, orange, yellow, or white shading indicating high, intermediate, low, or no detectable binding,

respectively. EC_{50} values greater than 10,000 ng/mL are indicated by the > symbol. One experiment representative of two independent experiments is shown. (C) Heat map showing the neutralization capacity of HEPC3, HEPC74, AR3C and their germline precursors measured using a panel of genotype 1 HCVpp. IC_{50} values for each virus-mAb combination are shown, with IC_{50} values greater than 10,000 ng/mL indicated by the > symbol. See also Figure S6, S7.

KEY RESOURCES TABLE

REAGENT or RESOURCE	SOURCE	IDENTIFIER
Chemicals, Peptides, and Recombinant Proteins		
PEGRx HT	Hampton Research	Cat#HR12–086
PEG/Ion HT	Hampton Research	Cat#HR2–139
JCSG-plus™ HT-96	Molecular Dimensions	Cat#MD1–40
Fomblin® Y oil	Sigma	Cat#317942
1-Step™ Ultra TMB-ELISA Substrate Solution	Thermo Fisher Scientific	Cat#34028
Kifunensine	Sigma	Cat#K1140
Goat Anti-Human IgG-HRP	SouthernBiotech	Cat#2040–05
HEPC3	(Bailey et al., 2017)	N/A
HEPC74	(Bailey et al., 2017)	N/A
HEPC46	(Bailey et al., 2017)	N/A
AR3C	(Kong et al., 2013)	N/A
Experimental Models: Cell Lines		
HEK293–6E	National Research Council of Canada	Cat#11565
Hep3B2.1–7	ATCC	Cat# HB-8064
Recombinant DNA		
pTT5 mammalian expression vector (used to express all IgGs and Fabs)	National Research Council of Canada	N/A
Software and Algorithms		
Pymol	Schrödinger, 2011	RRID:SCR_000305
Phenix	(Adams et al., 2010)	https://www.phenix-online.org
Coot	(Emsley and Cowtan, 2004)	http://www2.mrc-lmb.cam.ac.uk/personal/pemsley/coot/
PDBePISA	(Krissinel and Henrick, 2007)	http://www.ebi.ac.uk/pdbe/pisa/
HIV Antibody Database (used to calculate Fab rotation angles)	(West et al., 2013)	https://itunes.apple.com/us/app/hiv-antibody-database/id1232472905?mt=8
Deposited Data		
HEPC3 coordinates	PDB	6MED
HEPC74 coordinates	PDB	6MEE
AR3C coordinates	PDB	6MEF
HEPC46 coordinates	PDB	6MEG
HEPC74-E2ecto coordinates	PDB	6MEH
HEPC3-E2ecto coordinates	PDB	6MEI
HEPC3-E2ecto-HEPC46 coordinates	PDB	6MEJ
HEPC3-E2core-HEPC46 coordinates	PDB	6MEK
Other		
Superdex 200 Increase 10/300 GL	GE Healthcare	Cat#17517501

REAGENT or RESOURCE	SOURCE	IDENTIFIER
Chemicals, Peptides, and Recombinant Proteins		
HisTrap FF column	GE Healthcare	Cat#17531901
HiTrap Protein A HP column	GE Healthcare	Cat#17040301
StrepTrap HP column	GE Healthcare	Cat#28907547
HCV 1a53 strain E1E2 sequence	GenBank	FJ828970.1
HCV 1b09 strain E1E2 sequence	GenBank	KJ187984.1